

Density Functional Theory Study on the Nucleation and Growth of Pt_n Clusters on γ-Al₂O₃(001) Surface

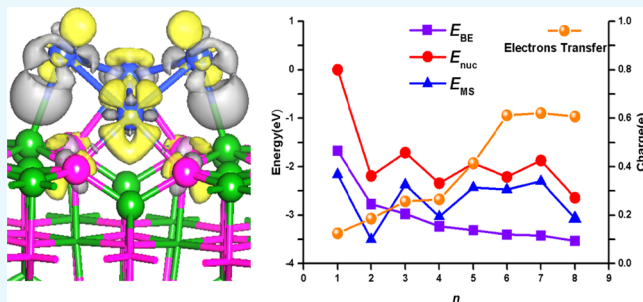
Yue Wang,[†] Bo Xiang,[†] Hua-Qing Yang,^{*,†} and Chang-Wei Hu,[‡]

[†]College of Chemical Engineering, Sichuan University, Chengdu, Sichuan 610065, P. R. China

[‡]Key Laboratory of Green Chemistry and Technology, Ministry of Education, College of Chemistry, Sichuan University, Chengdu, Sichuan 610064, P. R. China

Supporting Information

ABSTRACT: Little is known about the detailed structural information at the interface of Pt_n cluster and γ-Al₂O₃(001) surface, which plays an important role in the dehydrogenation and cracking of hydrocarbons. Here, the nucleation and growth of Pt_n ($n = 1\text{--}8, 13$) clusters on a γ-Al₂O₃(001) surface have been examined using density functional theory. For the most stable configuration Pt_n/γ-Al₂O₃(001) ($n = 1\text{--}8, 13$), Pt_n clusters bond to the γ-Al₂O₃(001) surface through Pt–O and Pt–Al bonds at the expense of electron density of the Pt_n cluster. With the increase in the Pt_n cluster size, both the metal–support interaction and the nucleation energies exhibit an odd–even oscillation pattern, which are lower for an even Pt_n cluster size than those for its adjacent odd ones. Both the metal–surface and metal–metal interactions are competitive, which control the nanoparticle morphology transition from two-dimension (2D) to three-dimension (3D). On the γ-Al₂O₃(001) surface, when the metal–support interaction governs, smaller clusters such as Pt₁, Pt₂, Pt₃, and Pt₄ prefer a planar 2D nature. Alternatively, when the metal–metal interaction dominates, larger clusters such as Pt₅, Pt₆, Pt₇, Pt₈, and Pt₁₃ exhibit a two-layer structure with one or more Pt atoms on the top layer not interacting directly with the support. Herein, the Pt₄ cluster is the most stable 2D structure; Pt₅ and Pt₆ clusters are the transition from the 2D to the 3D structure; and the Pt₇ cluster is the smallest 3D structure.



1. INTRODUCTION

In recent years, Pt-based catalysts have attracted particular attention with respect to their catalytic performance toward the dehydrogenation and cracking of hydrocarbons, ranging from energy-efficient and environmentally friendly synthesis strategies to the replacement of petrochemical feedstocks by abundant small alkanes.^{1–3} In this heterogeneous catalysis, metal–support interaction is of great importance because it can influence the heterostructural properties of metallic nanoparticles (NPs), that is, the degree of dispersion, morphology, and nucleation. Therefore, a fundamental question in catalytic research is how to exploit metal–support interaction to optimize the NP morphology to achieve good catalytic activity, selectivity, and sintering suppression.

An important factor in Pt-based catalysis is the size effect of NPs. This has been nicely corroborated for the catalytic dehydrogenation of hydrocarbons by Pt_n^{0/+} cluster. Here, we discuss several typical examples. Experimentally, it was discovered earlier that the neutral Pt_n clusters ($n \leq 24$) can efficiently activate CH₄, whereas Pt_n ($n = 2\text{--}5$) clusters are more reactive than the mononuclear platinum atom.⁴ Later, theoretically, it was reported that the neutral clusters Pt₂, Pt₃, and Pt₄ can activate the first C–H bond of CH₄ with small barriers, accompanied by the breakage of the second C–H bond in CH₄ as the rate-determining step.^{5–7} More recently,

we have studied the competitive activation mechanism of C–H and C–C bonds in C₂H₆ and/or C₃H₈ catalyzed by the Pt_n ($n = 1, 2$, and 4) cluster^{8–12} and explained why the C–H insertion product is experimentally observed while the C–C insertion product is not formed in observable quantity^{8,9} and why both Pt₂ and Pt₄ clusters exhibit more promising catalytic performance toward C₂H₆ activation compared with the Pt atom.^{10,12} These experimental and theoretical studies emphasize that the size of transition-metal clusters plays an important role in the catalytic reactivity.

Another key factor in the Pt-based catalysis is the metal–support interaction that plays a crucial role in the deposition of size-selected metal clusters onto a well-defined support surface. Tremendous progress has been made in this direction. Experimentally, Vajda et al. deposited size-selected Pt_{8–10} clusters on a porous aluminum oxide support and found that they are over 40 times more active for the oxidative dehydrogenation of propane than the conventional catalyst, while retaining the high selectivity to propylene.² Theoretically, several studies were devoted to understanding the growth of Pt nanoclusters on supports such as α-Al₂O₃(0001),¹³ γ-

Received: March 22, 2017

Accepted: June 21, 2017

Published: July 7, 2017

$\text{Al}_2\text{O}_3(100)$,¹⁴ $\gamma\text{-Al}_2\text{O}_3(110)$,¹⁵ anatase $\text{TiO}_2(101)$,^{16–18} rutile $\text{TiO}_2(110)$,¹⁹ graphene,^{20–23} ceria $\text{CeO}_2(111)$,²⁴ and boron nitride (BN).²⁵ The relatively large cohesive energy of Pt makes it highly probable that atomic layer deposition (ALD) will produce a dispersion of Pt NPs and formation of 3D islands rather than thin films, as was found previously on several supports.^{13,16–18,24} However, the smallest cluster size of NPs, above which the growth transforms from two-dimension (2D) to three-dimension (3D), is generally the result of a delicate interplay between the metal–metal and metal–substrate interactions. These experimental and theoretical studies show that the support plays a key role in the nucleation and morphology of the Pt_n cluster.

$\gamma\text{-Al}_2\text{O}_3$ is extensively used as the support because of its acid–base properties and mechanical and thermal resistance and plays an essential role in the catalytic performance. It has been experimentally and theoretically reported that about 70% of the exposed surface of γ -alumina can be represented by a (110) termination with three-coordinated and four-coordinated Al atoms.^{26,27} However, this surface is generally expected to be strongly hydrated, even at high temperatures. Therefore, no low-coordinated ions of the $\text{Al}_2\text{O}_3(110)$ framework are available for the interaction with the adsorbed transition-metal particles.²⁸ The remaining 30% of the exposed surface are expected to feature mainly (111) and (001) terminations.^{26,27} The $\gamma\text{-Al}_2\text{O}_3(001)$ surface is dominated by five-coordinated Al atoms, with some four-coordinated Al atoms, both of which are expected to be weaker Lewis acids.²⁹ The $\gamma\text{-Al}_2\text{O}_3(001)$ surface, as the most stable surface, is assumed to interact mostly with the supported NPs through low-coordinated anions of the support.^{28–30} So far, only limited study has focused on the nucleation and growth of NPs on the $\gamma\text{-Al}_2\text{O}_3(001)$ surface.^{31,32} However, the nucleation and morphology of the Pt_n cluster on the $\gamma\text{-Al}_2\text{O}_3(001)$ surface is still not well-understood.

In this study, we will examine the stability and nucleation of different small Pt_n ($n = 1–8$) clusters on the $\gamma\text{-Al}_2\text{O}_3(001)$ surface by the density functional theory (DFT) method. The goals are to find answers to the following four questions in particular: (1) Which is the preferred adsorption configuration? (2) How do the Pt_n clusters bond to the $\gamma\text{-Al}_2\text{O}_3(001)$ surface? (3) How does the metal–support interaction depend upon size? and (4) Is there a transition from a planar to a 3D structure and where does it occur?

2. RESULTS AND DISCUSSION

2.1. Gas-Phase Pt_n Clusters. To understand the growth behavior of Pt_n cluster on the $\gamma\text{-Al}_2\text{O}_3(001)$ surface, it is necessary to first describe the geometries and energies of gas-phase Pt_n clusters. For the gas-phase Pt_n clusters, 1D, 2D, and 3D structures are considered, and only the energetically preferred geometries and the binding energy (E_{BE}) are depicted in Figure S1. As shown in Figure S1, the Pt–Pt distances in the clusters are shorter than that in the bulk structure (2.775 Å), which increase from 2.401 to 2.672 Å with $n = 1–6$, decrease from 2.672 to 2.609 Å with $n = 6–7$, and then increase from 2.609 to 2.621 Å with $n = 7–8$, far from the bulk value (2.775 Å). The calculated bond distance of the dimer is 2.401 Å, which is close to the experimental value of 2.333 Å.⁴¹ The degree of bond contraction relative to the bulk follows an approximate $n^{-1/3}$ ($n = 1–6$) relationship,⁴² which has been characterized experimentally for the Pt cluster by extended X-ray absorption fine structure (EXAFS).⁴³ As expected, the binding energy increases as the cluster size increases because of increased

atomic coordination. The difference between the binding energy of a cluster and the bulk binding energy scales approximately as $n^{-1/3}$ ($n = 1–8$), which is in good agreement with the reported result.⁴²

2.2. Adsorption of $\text{Pt}_1\text{-}\text{Pt}_4$ Clusters—2D Growth. The side and top views of $\gamma\text{-Al}_2\text{O}_3(001)$ are presented in Figure 1.

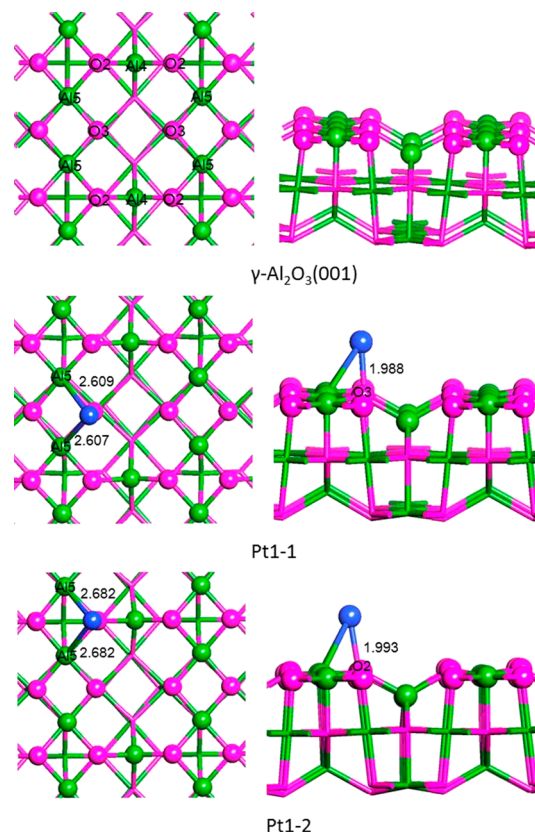


Figure 1. Top and side views of the $\gamma\text{-Al}_2\text{O}_3(001)$ and monomer adsorption configurations on the $\gamma\text{-Al}_2\text{O}_3(001)$ surface. O, Al, and Pt atoms are shown as pink, green, and blue spheres, respectively. The bond length is in Å.

As shown in Figure 1, there are two types of Al atoms: four-coordinated and five-coordinated, denoted as Al4 and Al5, respectively. Moreover, there are two types of O atoms: one connecting with one four-coordinated Al atom and two five-coordinated Al atoms and another interacting with three five-coordinated Al atoms, denoted as O2 and O3. By Hirshfeld analysis, the charges of Al4, Al5, O2, and O3 are determined to be +0.562, +0.493, -0.334, and -0.366, respectively. Taking into account the geometrical structure, Al4 is expected to be far from the metal cluster, as it is located in the hollow site. In addition, three possible adsorption sites can be easily recognized, namely, Al5, O2, and O3. Table 1 summarizes the relevant structural parameters and adsorption energies for the lowest energy configurations that are most relevant to the nucleation process.

2.2.1. (Pt_1). For the adsorption of a single Pt atom on the $\gamma\text{-Al}_2\text{O}_3(001)$ surface, the obtained most stable two configurations are depicted in Figure 1.

As shown in Table 1 and Figure 1, the preferential adsorption configuration is the atop-O3 site (Pt1-1) with a binding energy of -1.67 eV/atom, which is 0.27 eV more stable than the atop-O2 site (Pt1-2) with a binding energy of -1.40 eV/atom.

Table 1. Relative Energies (E_R , eV), Binding Energies (E_{BE} , eV), $\gamma\text{-Al}_2\text{O}_3(001)$ Deformation Energies $\Delta E_{def,\text{Al}_2\text{O}_3}$ (eV), Cluster Deformation Energies ($\Delta E_{def,\text{Pt}_n}$, eV), Metal–Support Interaction Energies (E_{MS} , eV), Metal–Metal Bond Energy ($\Delta E_{bond,\text{Pt}_n}$, eV), Bond Length (Å), and Electron Transfer (ET, e) from the Pt_n Cluster to the $\gamma\text{-Al}_2\text{O}_3(001)$ Surface for the Corresponding Configurations^a

configuration	E_R	E_{BE}	$\Delta E_{def,\text{Al}_2\text{O}_3}$	$\Delta E_{def,\text{Pt}_n}$	E_{MS}	$\Delta E_{bond,\text{Pt}_n}$	$\text{Pt-Al } \bar{l}$	$\text{Pt-O } \bar{l}$	$\text{Pt-Pt } \bar{l}$	ET
Pt1-1	0.00	-1.67	0.49	0.00	-2.16	0.00	2.608	1.988		0.125
Pt1-2	0.27	-1.40	0.51	0.00	-1.91	0.00	2.682	1.993		0.107
Pt2-1	0.00	-2.77	2.22	0.10	-3.50	-1.49	2.604	2.085	2.521	0.186
Pt2-2	1.66	-1.94	1.18	0.19	-1.68	-1.44		2.483	2.476	0.147
Pt3-1	0.00	-2.97	1.50	0.10	-2.37	-2.10	2.545	2.159	2.600	0.257
Pt3-2	0.01	-2.97	1.18	0.00	-2.02	-2.13		2.130	2.550	0.069
Pt4-1	0.00	-3.23	2.17	0.06	-3.03	-2.37	2.565	2.297	2.606	0.265
Pt4-2	0.70	-3.05	1.72	0.11	-2.39	-2.39	2.631	2.163	2.654	0.157
Pt5-1	0.00	-3.31	1.70	0.23	-2.43	-2.57	2.650	2.073	2.578	0.415
Pt5-2	0.23	-3.26	2.44	0.52	-3.19	-2.51	2.611	2.241	2.614	0.380
Pt6-1	0.00	-3.40	1.75	0.67	-2.47	-2.68	2.624	2.081	2.545	0.612
Pt6-2	0.08	-3.39	1.73	0.46	-2.39	-2.73	2.566	2.107	2.615	0.360
Pt7-1	0.00	-3.42	1.68	0.22	-2.30	-2.81	2.647	2.090	2.553	0.621
Pt7-2	0.05	-3.42	2.01	0.38	-2.52	-2.91	2.568	2.174	2.593	0.251
Pt8-1	0.00	-3.53	2.44	0.96	-3.07	-2.90	2.608	2.105	2.582	0.607
Pt8-2	0.20	-3.51	2.09	0.56	-2.55	-3.06	2.625	2.348	2.627	0.439
Pt13-1	0.00	-3.76	2.21	0.80	-2.66	-3.31	2.653	2.164	2.623	0.661

^aAverage bond lengths \bar{l} with a threshold of 3.0 Å

Binding energies of the monomers and ordering of the different adsorption sites can be rationalized by examining the optimum structures and electronic properties. In the Pt1-1 configuration, the Pt atom binds to O3 with a bond length of 1.988 Å and binds to two Al5 atoms with the average bond length of 2.608 Å. Similarly, in the Pt1-2 configuration, the Pt atom connects to O2 with a bond length of 1.993 Å and binds to two Al5 atoms with equal bond lengths of 2.682 Å. It is apparent that there are two Pt–Al5 bonds and one Pt–O3 bond in Pt1-1, and there are two Pt–Al5 bonds and one Pt–O2 bond in Pt1-2. The shorter bond lengths of Pt–O and Pt–Al make Pt1-1 more stable than Pt1-2. This can be ascribed to the fact that O3 (-0.366) is charged more negatively than O2 (-0.334) on a pristine $\gamma\text{-Al}_2\text{O}_3(001)$ surface. Charge analysis shows that there is an electron transfer of 0.125e from Pt to $\gamma\text{-Al}_2\text{O}_3(001)$ in Pt1-1 and an electron transfer of 0.107e in Pt1-2. The order of ET accords stability to the two configurations. It is indicated that the atop-O3 site is more favorable than the atop-O2 one. That is to say that the Pt atom interacts more firmly with O3 than O2. This result may be ascribed to the more negative charge on O3 than that on O2.

2.2.2. (Pt)₂. On the basis of Pt₁/ $\gamma\text{-Al}_2\text{O}_3(001)$ configurations, the introduction of the second Pt atom may form four possible configurations. For the adsorption of a Pt₂ cluster on the $\gamma\text{-Al}_2\text{O}_3(001)$ surface, the obtained most stable two configurations are depicted in Figure 2.

As shown in Table 1 and Figure 2, the four stable configurations have a relative stabilization energy within 1.67 eV (see Table S1). The preferential adsorption configuration is Pt2-1 with a binding energy of -2.77 eV/atom, which is about 0.83 eV more stable than Pt2-2, Pt2-3, and Pt2-4, which have an equal binding energy of about -1.94 eV/atom. Let us inspect their optimum structure and electronic properties. As shown in Table 1 and Figure 2, in the Pt2-1 configuration, the Pt dimer is positioned nearly across the O3–O3 pair; whereas one Pt atom binds to two O3 atoms with the average bond length of 2.085 Å, another Pt atom links to two Al5 atoms with

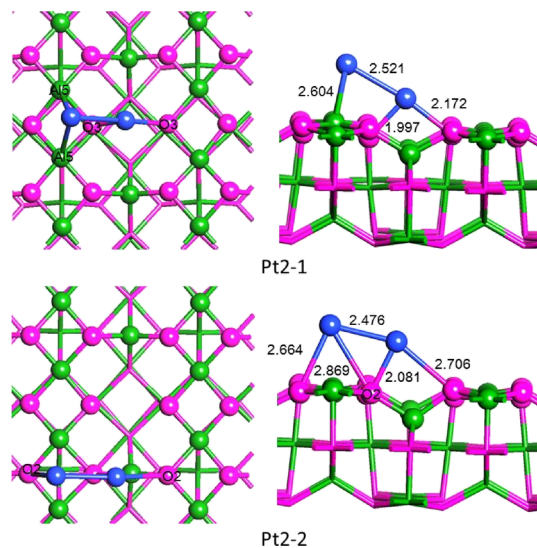


Figure 2. Top and side views of the dimer adsorption configurations on the $\gamma\text{-Al}_2\text{O}_3(001)$ surface. The bond length is in Å.

equal bond lengths of 2.604 Å. Next, in the Pt2-2 configuration, the Pt dimer is adsorbed across the O2–O2–O2 pair, whereas each Pt atom connects to two O2 atoms with the average bond length of 2.483 Å. Deformation energies mainly embody at the $\gamma\text{-Al}_2\text{O}_3(001)$ surface in the range of 2.22–0.64 eV, whereas they vary little at the Pt₂ cluster in the range of 0.20–0.04 eV. However, the Pt–Pt bond length is elongated by about 0.07–0.28 Å. By charge analysis, there is a charge transfer of 0.186e from Pt₂ to $\gamma\text{-Al}_2\text{O}_3(001)$ in Pt2-1 and a charge transfer of 0.147e in Pt2-2.

2.2.3. (Pt)₃. In the light of Pt₃/ $\gamma\text{-Al}_2\text{O}_3(001)$ configurations, the introduction of the third Pt atom may result in six possible configurations. For the adsorption of a Pt₃ cluster on the $\gamma\text{-Al}_2\text{O}_3(001)$ surface, the obtained most stable two configurations are depicted in Figure 3. Six stable configurations are

obtained with the relative energy within about 1.10 eV (see Table S1).

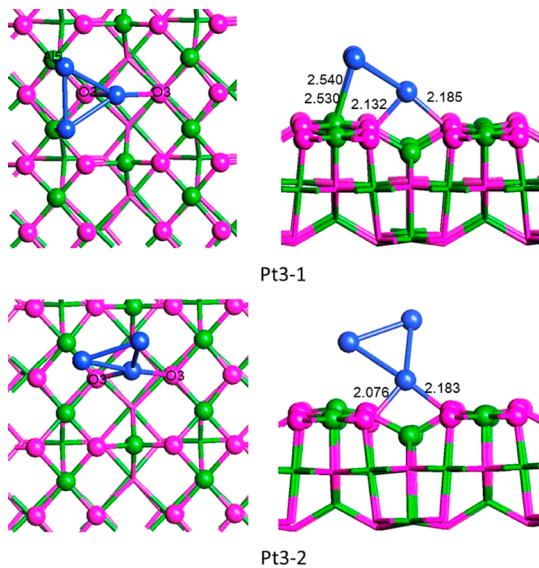


Figure 3. Top and side views of the trimer adsorption configurations on the $\gamma\text{-Al}_2\text{O}_3(001)$ surface. The bond length is in Å.

As shown in Table 1 and Figure 3, the lowest energy configurations are Pt3-1 and Pt3-2 with an equal binding energy of -2.97 eV/atom. Now, it is necessary to investigate their optimum structure and electronic properties. As shown in Table 1 and Figure 3, in Pt3-1, the Pt_3 triangular plane is parallel to the $\gamma\text{-Al}_2\text{O}_3(001)$ surface; whereas one Pt atom binds to one O3 atom with the bond length of 2.159 Å, the other two Pt atoms link to two Al5 atoms with equal bond lengths of 2.545 Å. Then, in Pt3-2, the Pt_3 triangular plane is perpendicular to the $\gamma\text{-Al}_2\text{O}_3(001)$ surface through the vertex of the triangle; whereas one Pt atom connects to two O3 atoms with the average bond length of 2.130 Å, the other two Pt atoms are out of the $\gamma\text{-Al}_2\text{O}_3(001)$ substrate. Hence, there are two Pt–Al5 bonds and one Pt–O3 bond in Pt3-1, and there are two Pt–O3 bonds in Pt3-2. It is indicated that the synergism of Pt with both Al5 and O3 makes the Pt3-1 configuration more stable. Deformation energies mainly reflect at the $\gamma\text{-Al}_2\text{O}_3(001)$ surface in the range of 1.50 – 0.56 eV, with hardly any at the Pt3 cluster. However, the average Pt–Pt bond length is elongated by about 0.01 – 0.07 Å. In the light of charge analysis, there is a charge transfer of $0.257e$ from Pt3 to $\gamma\text{-Al}_2\text{O}_3(001)$ in Pt3-1 and a charge transfer of $0.069e$ in Pt3-2.

2.2.4. (Pt)₄. According to the Pt3/ $\gamma\text{-Al}_2\text{O}_3(001)$ configurations, the introduction of the fourth Pt atom may bring about eight possible configurations. For the adsorption of a Pt4 cluster on the $\gamma\text{-Al}_2\text{O}_3(001)$ surface, the obtained most stable two configurations are depicted in Figure 4. Eight stable configurations are obtained with the relative stabilization energy within about 1.21 eV (see Table S1).

As shown in Table 1 and Figure 4, the most stable configuration is Pt4-1 with a binding energy of -3.23 eV/atom, followed by Pt4-2 with an almost equal binding energy of -3.04 eV/atom. Next, let us discuss their optimum structure and electronic properties. As shown in Table 1 and Figure 4, in Pt4-1, the Pt4 cluster is adsorbed as a symmetric boatlike species on the $\gamma\text{-Al}_2\text{O}_3(001)$ surface; whereas one Pt atom links to two O3 atoms and the second Pt atom links to two O2 atoms.

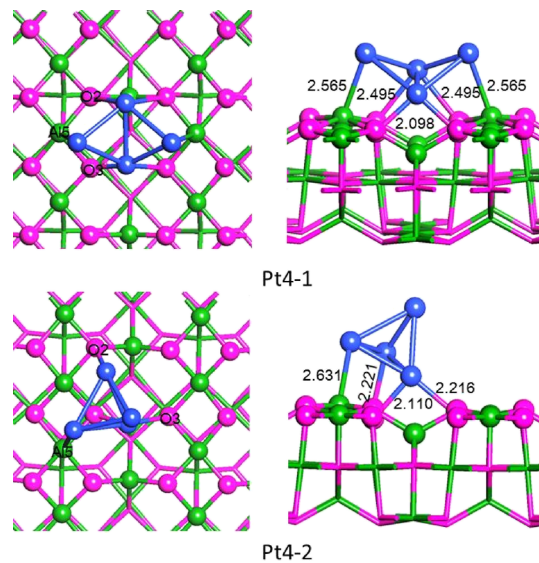


Figure 4. Top and side views of the tetramer adsorption configurations on the $\gamma\text{-Al}_2\text{O}_3(001)$ surface. The bond length is in Å.

atoms, with the average bond length of 2.297 Å, the remaining two Pt atoms link to two Al5 atoms with equal bond lengths of 2.565 Å. Then, in Pt4-2, the Pt4 tetrahedral pyramid is deposited on the $\gamma\text{-Al}_2\text{O}_3(001)$ surface; whereas one Pt atom connects to two O3 atoms, the second Pt atom connects to one O2 atom, the third Pt atom connects to one Al5 atom, and the fourth one is in the second layer, with average bond lengths of 2.163 Å for Pt–O and 2.631 Å for Pt–Al. Hence, there are two Pt–Al5 bonds, two Pt–O3 bonds, and two Pt–O2 bonds in Pt4-1, and there are one Pt–Al5 bond, two Pt–O3 bonds, and one Pt–O2 bond in Pt4-2. In view of the charge analysis, there is a charge transfer of $0.256e$ from Pt4 to $\gamma\text{-Al}_2\text{O}_3(001)$ in Pt4-1 and a charge transfer of $0.157e$ in Pt4-2.

In addition, the temperature effect was taken into account on the size and shape of the typical Pt4 cluster on the $\gamma\text{-Al}_2\text{O}_3(001)$ surface, which may be the transition of 2D to 3D. The 2D Pt4-1 configuration is more stable than the 3D Pt4-2 configuration below 75 K, whereas the 3D Pt4-2 configuration is more stable than the 2D Pt4-1 configuration above 75 K (see Figure S12).

2.3. Adsorption of Pt₅ and Pt₆ Clusters—2D–3D Transition. **2.3.1. (Pt)₅.** In line with the Pt4/ $\gamma\text{-Al}_2\text{O}_3(001)$ configurations, the introduction of the fifth Pt atom may give eight possible configurations. For the adsorption of a Pt5 cluster on the $\gamma\text{-Al}_2\text{O}_3(001)$ surface, the obtained most stable two configurations are depicted in Figure 5. Eight stable configurations are obtained with the relative energy within about 1.18 eV (see Table S1).

As shown in Table 1 and Figure 5, the preferable lowest energy configuration is Pt5-1 with a binding energy of -3.31 eV/atom, followed by Pt5-2 with a binding energy of -3.26 eV/atom. Now, let us examine their optimum structure and electronic properties. As shown in Table 1 and Figure 5, in Pt5-1, one Pt atom attaches to two O3 atoms, three Pt atoms attach to three Al5 atoms, and the fifth Pt atom is in the second layer, with average bond lengths of 2.073 Å for Pt–O and 2.650 Å for Pt–Al. Afterward, in Pt5-2, one Pt atom connects to two O3 atoms, one Pt atom connects to one O2 atom, three Pt atoms connect to three Al5 atoms, with average bond lengths of 2.241 Å for Pt–O and 2.611 Å for Pt–Al. Hence, there are three Pt–Al5 bonds and two Pt–O3 bonds in Pt5-1, and there are three

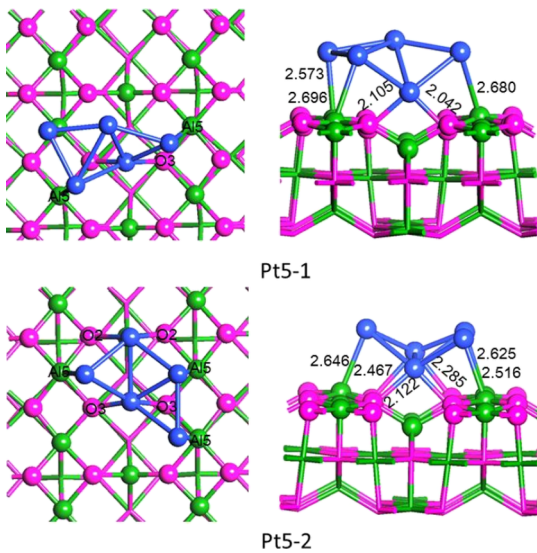


Figure 5. Top and side views of the pentamer adsorption configurations on the $\gamma\text{-Al}_2\text{O}_3(001)$ surface. The bond length is in Å.

Pt–Al5 bonds, two Pt–O3 bonds, and two Pt–O2 bonds in Pt5-2. The reason that Pt5-2 is 0.23 eV higher in energy than Pt5-1 may be attributed to the longer bond lengths of Pt–O and Pt–Pt. In view of the charge analysis, there is a charge transfer of 0.415e from Pt₅ to $\gamma\text{-Al}_2\text{O}_3(001)$ in Pt5-1 and a charge transfer of 0.380e in Pt5-2.

2.3.2. (Pt)₆. On the basis of the Pt₅/ $\gamma\text{-Al}_2\text{O}_3(001)$ configurations, the introduction of the sixth Pt atom may produce six possible configurations. For the adsorption of a Pt₆ cluster on the $\gamma\text{-Al}_2\text{O}_3(001)$ surface, the obtained most stable two configurations are depicted in Figure 6. Eight stable configurations are obtained with the relative energy within about 0.67 eV (see Table S1).

As shown in Table 1 and Figure 6, the most stable configuration is Pt6-1 with a binding energy of −3.40 eV/atom, followed by Pt6-2 with a binding energy of −3.39 eV/atom. Now, let us look into their optimum structure and electronic properties. As shown in Table 1 and Figure 6, in Pt6-1, one Pt

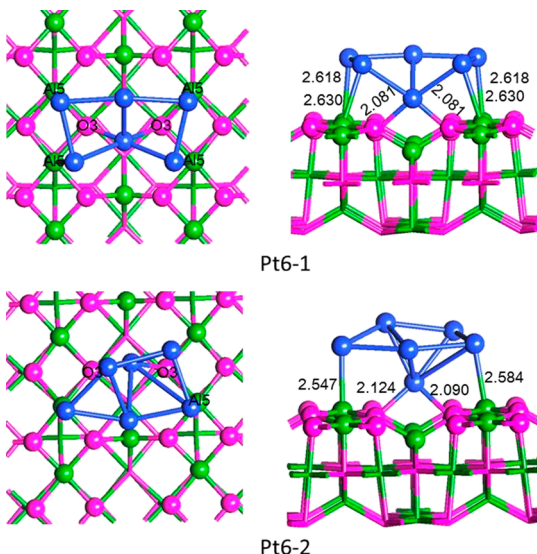


Figure 6. Top and side views of the hexamer adsorption configurations on the $\gamma\text{-Al}_2\text{O}_3(001)$ surface. The bond length is in Å.

atom binds to two O3 atoms, four Pt atoms bind to four Al5 atoms, and the sixth one is in the second layer, with average bond lengths of 2.081 Å for Pt–O and 2.624 Å for Pt–Al. In addition, in Pt6-2, one Pt atom links to two O3 atoms, two Pt atoms link to two Al5 atoms, and the other three Pt atoms are in the second layer, with average bond lengths of 2.107 Å for Pt–O and 2.566 Å for Pt–Al. It is obvious that Pt6-2 is only 0.08 eV higher in energy than Pt6-1. Such a low difference in energy makes them to coexist thermodynamically. It is indicated that the 2D–3D transition may take place in the Pt₆ cluster. In a word, there are four Pt–Al5 bonds and two Pt–O3 bonds in Pt6-1, and there are two Pt–Al5 bonds and two Pt–O3 bonds in Pt6-2. Considering the charge analysis, there is a charge transfer of 0.612e from Pt₆ to $\gamma\text{-Al}_2\text{O}_3(001)$ in Pt6-1 and a charge transfer of 0.360e in Pt6-2.

2.4. Adsorption of Pt₇, Pt₈, and Pt₁₃ Clusters—3D Growth. **2.4.1. (Pt)₇.** In the light of the Pt₆/ $\gamma\text{-Al}_2\text{O}_3(001)$ configurations, the introduction of the seventh Pt atom may form eight possible configurations. For the adsorption of a Pt₇ cluster on the $\gamma\text{-Al}_2\text{O}_3(001)$ surface, the obtained most stable two configurations are depicted in Figure 7. Eight stable configurations are obtained with the relative stabilization energy within about 1.37 eV (see Table S1).

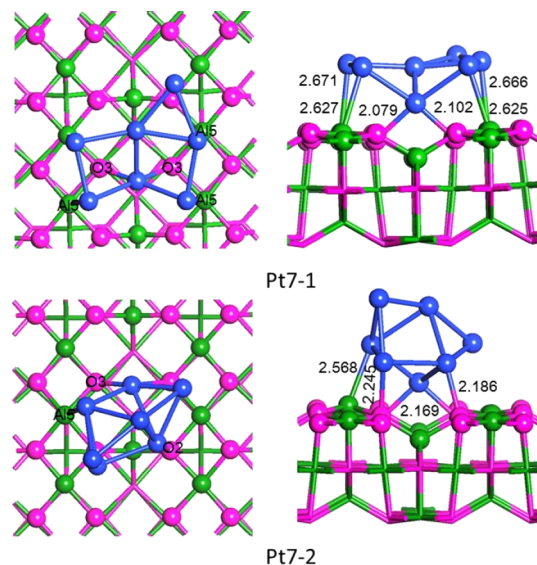


Figure 7. Top and side views of the heptamer adsorption configurations on the $\gamma\text{-Al}_2\text{O}_3(001)$ surface. The bond length is in Å.

As shown in Table 1 and Figure 7, the preferable stable configuration is Pt7-1 with a binding energy of −3.42 eV/atom, followed by Pt7-2 with a binding energy of −3.42 eV/atom. Now, let us inspect their optimum structure and electronic properties. As shown in Table 1 and Figure 7, in Pt7-1, one Pt atom links to two O3 atoms, four Pt atoms link to four Al5 atoms, and the other one is in the second layer, with average bond lengths of 2.090 Å for Pt–O and 2.647 Å for Pt–Al. Next, in Pt7-2, one Pt atom binds to two O3 atoms, two Pt atoms bind to two O2 atoms, one Pt atom binds to the Al5 atom, and the other three Pt atoms are in the second layer, with average bond lengths of 2.174 Å for Pt–O and 2.568 Å for Pt–Al. Moreover, there is a close relative energy between Pt7-1 and Pt7-2, indicating that they should coexist thermodynamically. In short, there are four Pt–Al5 bonds and two Pt–O3 bonds in Pt7-1, and there are one Pt–Al5 bond, two Pt–O3 bonds, and

two Pt–O₂ bonds in Pt7-2. Concerning the charge analysis, there is a charge transfer of 0.621e from Pt₇ to γ-Al₂O₃(001) in Pt7-1 and a charge transfer of 0.251e in Pt7-2.

As depicted in Figure 7, the growth of a Pt heptamer island differs from the previous cases. For the Pt heptamer, the preferable lowest energy configuration is 3D in nature with five Pt atoms in the lower layer and two Pt atoms in the upper layer, whereas for the previous Pt_n/γ-Al₂O₃(001) ($n < 7$) heterostructures with at most one Pt atom in the second layer. For comparison, the growth of Pt₈ on rutile TiO₂(110) and the growth of Pt₅ on Mo₂S(001) showed a 3D nature with more than one atom residing in the second layer.^{18,44}

2.4.2. (Pt)₈. In view of the Pt₇/γ-Al₂O₃(001) configurations, the introduction of the eighth Pt atom may form four possible configurations. For the adsorption of a Pt₈ cluster on the γ-Al₂O₃(001) surface, the obtained most stable two configurations are depicted in Figure 8. Four stable configurations are obtained with the relative stabilization energy within about 2.21 eV (see Table S1).

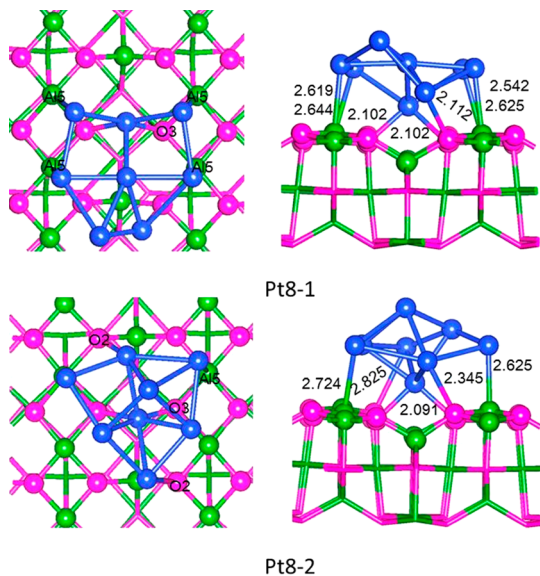


Figure 8. Top and side views of the octamer adsorption configurations on the γ-Al₂O₃(001) surface. The bond length is in Å.

As shown in Table 1 and Figure 8, the preferable lowest energy configuration is Pt8-1 with a binding energy of -3.53 eV/atom, followed by Pt8-2 with a binding energy of -3.51 eV/atom. Next, let us examine their optimum structure and electronic properties. As shown in Table 1 and Figure 8, in Pt8-1, one Pt atom links to two O₃ atoms, one Pt atom links to one O₂ atom, four Pt atoms link to four Al₅ atoms, and the other two Pt atoms are in the second layer, with average bond lengths of 2.105 Å for Pt–O and 2.608 Å for Pt–Al. Alternatively, in Pt8-2, one Pt atom binds to two O₃ atoms, two Pt atoms link to two O₂ atoms, two Pt atoms link to two Al₅ atoms, and the other three Pt atoms are in the second layer, with average bond lengths of 2.348 Å for Pt–O and 2.625 Å for Pt–Al. In addition, there are four Pt–Al₅ bonds, two Pt–O₃ bonds, and one Pt–O₂ bond in Pt8-1, and there are two Pt–Al₅ bonds, two Pt–O₃ bonds, and two Pt–O₂ bonds in Pt8-2. In view of the charge analysis, there is a charge transfer of 0.607e from Pt₈ to γ-Al₂O₃(001) in Pt8-1 and a charge transfer of 0.439e in Pt8-2, which may reflect the stability of the two configurations.

2.4.3. (Pt)₁₃. Because the Pt₁₃ cluster exhibits the highest stability among small clusters because of its “magic number” on various substrates, such as defective BN nanosheet²⁵ or defective graphene,^{45–47} it is very necessary to examine the adsorption of the Pt₁₃ cluster on the γ-Al₂O₃(001) surface. On the basis of the growth trend of Pt_n ($n = 1–8$) on the γ-Al₂O₃(001) surface, the most stable 3D configuration of Pt₁₃/γ-Al₂O₃(001) was designed. For the adsorption of a Pt₁₃ cluster on the γ-Al₂O₃(001) surface, the obtained stable configuration is depicted in Figure 9.

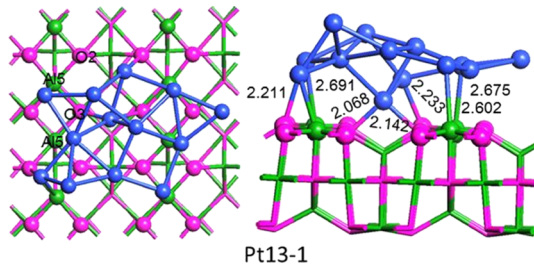


Figure 9. Top and side views of the Pt₁₃ adsorption configuration on the γ-Al₂O₃(001) surface. The bond length is in Å.

As shown in Table 1 and Figure 9, the preferable lowest energy configuration is Pt13-1 with a binding energy of -3.76 eV/atom. In Pt13-1, one Pt atom links to two O₃ atoms, two Pt atoms link to one O₂ atom, four Pt atoms link to four Al₅ atoms, and the other six Pt atoms are in the second layer, with average bond lengths of 2.164 Å for Pt–O and 2.653 Å for Pt–Al. Alternatively, in view of the charge analysis, there is a charge transfer of 0.661e from Pt₁₃ to γ-Al₂O₃(001).

2.5. Nucleation of the Pt_n Cluster on γ-Al₂O₃(001). As shown in Table 1, the deformation energy exists mainly on the γ-Al₂O₃(001) surface other than the Pt_n moiety. The trends of energy for the most stable configuration Pt_n/γ-Al₂O₃(001) ($n = 1–8$) are drawn in Figure 10.

As shown in Figure 10, with the increase in the Pt_n cluster size on the γ-Al₂O₃(001) surface, both the binding energy (E_{BE}) and the cohesive energy (E_{CE}) decrease and the difference between E_{CE} and E_{BE} gradually lessens. Furthermore, the

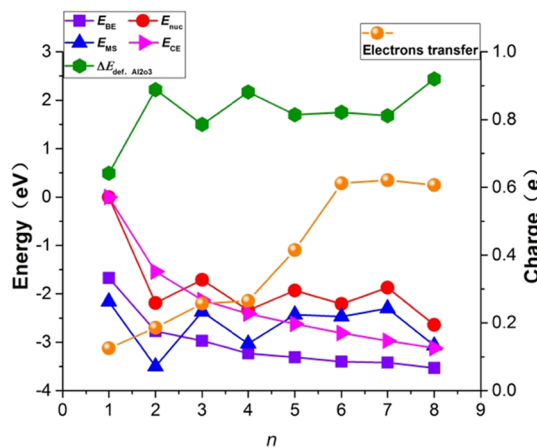


Figure 10. Binding energies (E_{BE}), nucleation energies (E_{nuc}), metal–support interaction energies (E_{MS}), cohesive energies (E_{CE}), γ-Al₂O₃(001) deformation energies ($\Delta E_{def, Al_2O_3}$), and a charge transfer for the most stable configuration of the Pt_n cluster on the γ-Al₂O₃(001) surface.

binding energies are smaller than cohesive energies. It is indicated that these clusters could cause diffusion. For the Pt₁ cluster on the $\gamma\text{-Al}_2\text{O}_3(001)$ surface, the diffusion barrier is calculated to be 0.16 eV (see Figure S10).

Alternatively, both the $\gamma\text{-Al}_2\text{O}_3(001)$ deformation ($\Delta E_{\text{def},\text{Al}_2\text{O}_3}$) and the metal–support interaction (E_{MS}) energies display an odd–even oscillation pattern. That is, the $\gamma\text{-Al}_2\text{O}_3(001)$ deformation energy ($\Delta E_{\text{def},\text{Al}_2\text{O}_3}$) increases with the increase in the Pt_{*n*} cluster size for both odd and even sizes, whereas it is higher for an even Pt_{*n*} cluster size than for its adjacent odd ones. Thereupon, the metal–support interaction (E_{MS}) energy decreases with the increase in the Pt_{*n*} cluster size for both odd and even sizes, whereas it is lower for an even size than for its adjacent odd sizes. That is to say, the odd–even oscillation pattern for $\Delta E_{\text{def},\text{Al}_2\text{O}_3}$ has an effect on the change in the metal–support interaction energy. Moreover, the nucleation energy (E_{nuc}) also shows an odd–even oscillation pattern, in which the nucleation energy of the even Pt_{*n*} cluster size is lower than that of its adjacent odd ones.

Furthermore, taking into account both the metal–support interaction (E_{MS}) and the metal–metal interaction ($\Delta E_{\text{bond},\text{Pt}_n}$) energies, one can see that the E_{MS} is lower than $\Delta E_{\text{bond},\text{Pt}_n}$ for $n = 1\text{--}4$ and higher for $n = 5\text{--}8$. Both the metal–surface and metal–metal interactions are competitive, which control the nanoparticle morphology transition from 2D to 3D. It is indicated that the cluster adopts a 2D nature for a small number of metal particles ($n < 5$) when the metal–support interaction governs, and the cluster gradually approaches a 3D morphology characteristic for a large number of metal particles ($n > 5$) when the metal–metal interaction dominates. These results can be echoed by the obtained stable geometric structures, as mentioned earlier. Combining with the results of geometric structures, one can conclude that Pt4-1 is the most stable 2D structure, Pt5-1 and Pt6-1 are the transition from 2D to 3D, and Pt7-1 is the smallest 3D structure with two Pt atoms in the second layer. Then, we will discuss the electronic properties for Pt4-1 and Pt7-1 configurations infra.

As shown in Figure 10, the ET from the Pt_{*n*} cluster to $\gamma\text{-Al}_2\text{O}_3(001)$ increases with the increase in the Pt_{*n*} cluster size number ($n = 1\text{--}6$) and varies little for $n = 6\text{--}8$. The DOS and the corresponding contour plots of the differential charge density for $\gamma\text{-Al}_2\text{O}_3(001)$, Pt1-1, Pt4-1, Pt7-1, and Pt13-1 are depicted in Figure 11.

As shown in Figure 11, for $\gamma\text{-Al}_2\text{O}_3(001)$, the DOS is characterized with a sharp peak from the O 2p orbital in the vicinity of the Fermi level (E_F) and two sharp peaks from the Al 3p orbital in the range of 4.0–6.0 eV. For Pt1-1, Pt4-1, Pt7-1, and Pt13-1, it is apparent that there is a sharp peak from the Pt 5d orbital near E_F , indicating strong hybridization between the Pt 5d orbital and the O 2p orbital. Furthermore, for Pt1-1 and Pt4-1, the O 2p orbital peaks around the E_F of the substrate are all shifted to low energy levels, whereas they hardly vary for Pt7-1 and Pt13-1. This phenomenon strengthens that there is a stronger metal–support interaction in Pt1-1 and Pt4-1 than that in Pt7-1 and Pt13-1. In addition, the Al 3p sharp peaks gradually decrease from $\gamma\text{-Al}_2\text{O}_3(001)$, Pt1-1, and Pt4-1 to Pt7-1 and disappear at Pt13-1. It is indicated that the Pt–Al interaction enhances by degrees with the increase in the Pt_{*n*} cluster size after the Pt_{*n*} cluster adsorption on $\gamma\text{-Al}_2\text{O}_3(001)$. This result is in good agreement with the geometric features as before. The above interactions of Pt–O and Pt–Al can be

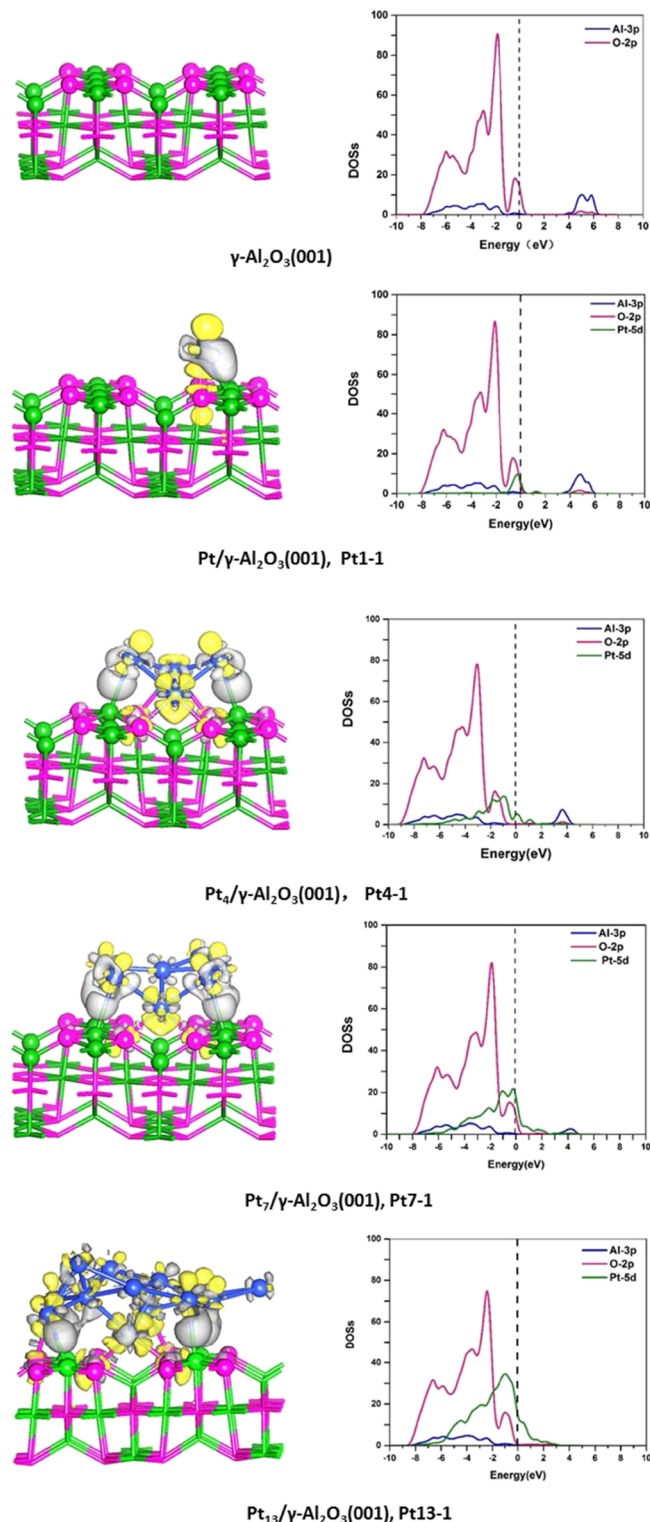


Figure 11. Density of states (DOS) and the corresponding contour plots of the differential charge density for $\gamma\text{-Al}_2\text{O}_3(001)$, Pt1-1, Pt4-1, Pt7-1, and Pt13-1. The Fermi level is set as zero in black dotted lines. The charge accumulation region is gray, and the charge depletion region is yellow. The isovalue is $0.05\text{e } \text{\AA}^{-3}$.

explained by the fact that there is a clear ET from the O²⁻ 2p occupied orbital to the Pt 5d* empty orbital and electron back donation from the Pt 5d occupied orbital to the Al³⁺ 3p* empty orbital in the deposited Pt_{*n*} cluster on the $\gamma\text{-Al}_2\text{O}_3(001)$ surface, as depicted in Figure 10. The net result of the ET makes the Pt_{*n*}

moiety positively charged and the $\gamma\text{-Al}_2\text{O}_3(001)$ moiety negatively charged. As shown in Figure 10, the electron density difference map reveals that some Pt orbitals are depleted upon adsorption on the surface. This depletion is balanced by an increase in the electron density of the Pt–O and/or Pt–Al bonds on the interfacial $\gamma\text{-Al}_2\text{O}_3(001)$.

3. CONCLUSIONS

The stability and nucleation of different small Pt_n ($n = 1\text{--}8, 13$) clusters on the $\gamma\text{-Al}_2\text{O}_3(001)$ surface have been examined using DFT. The following conclusions can be drawn from the present study.

There are 47 stable configurations $\text{Pt}_n/\gamma\text{-Al}_2\text{O}_3(001)$ ($n = 1\text{--}8$) obtained, in which the preferable adsorption configuration is ascertained for each size of the Pt_n cluster on the $\gamma\text{-Al}_2\text{O}_3(001)$ surface. For the most stable configuration $\text{Pt}_n/\gamma\text{-Al}_2\text{O}_3(001)$ ($n = 1\text{--}8, 13$), Pt_n clusters bond to the $\gamma\text{-Al}_2\text{O}_3(001)$ surface through Pt–O and Pt–Al bonds at the expense of the electron density of the Pt_n cluster.

On the $\gamma\text{-Al}_2\text{O}_3(001)$ surface, with the increase in the Pt_n cluster size, all $\gamma\text{-Al}_2\text{O}_3(001)$ deformations, metal–support interactions, and the nucleation energies exhibit an odd–even oscillation pattern. The metal–support interaction and the nucleation energies of an even Pt_n cluster size are lower than those of its adjacent odd ones, whereas the $\gamma\text{-Al}_2\text{O}_3(001)$ deformation energy of an even Pt_n cluster size is higher than that of its adjacent odd ones.

Both the metal–surface and metal–metal interactions are competitive, which control the nanoparticle morphology transition from 2D to 3D. On the $\gamma\text{-Al}_2\text{O}_3(001)$ surface, when the metal–support interaction predominates, smaller clusters such as Pt_1 , Pt_2 , Pt_3 , and Pt_4 exhibit a planar 2D nature. On the other hand, when the metal–metal interaction governs, larger clusters such as Pt_5 , Pt_6 , Pt_7 , Pt_8 , and Pt_{13} prefer a two-layer structure with one or more Pt atoms on the top layer not interacting with the support directly. Herein, the Pt_4 cluster is the most stable 2D structure, Pt_5 and Pt_6 clusters are the transition from 2D to 3D, and the Pt_7 cluster is the smallest 3D structure.

4. COMPUTATIONAL DETAILS

All calculations were performed by using Materials Studio 7.0 package.³³ The generalized gradient approximation (GGA) with the PW91 functional³⁴ is chosen together with the doubled numerical basis set and polarization basis set (DNP),³⁵ using the DMol³ program.³⁶ For the 5d transition-metal atom Pt, the scalar relativistic effects (density functional semicore pseudopotentials, DSPP) were considered for its core electrons.³⁷ The DNP basis sets have been successfully employed in the deposition of Pt clusters on the defective hexagonal BN (h-BN) sheets.²⁵ For the geometrical optimization, the forces imposed on each atom were converged to be less than 0.002 hartree/Å, the total energy was converged to be less than 1.0×10^{-6} hartree, and the displacement convergence was less than 5×10^{-3} Å. The k -point sampling scheme is the Monkhorst–Pack grid of $2 \times 2 \times 1$. A Fermi smearing of 0.005 hartree for orbital occupancy was used to improve the computational performance.

In addition, the properties of the isolated Pt_n clusters were calculated using a $15 \times 15 \times 15$ Å cubic unit cell. In the present study, bulk parameters of the $\gamma\text{-Al}_2\text{O}_3(001)$ surface model were first optimized according to the values of the Inorganic Crystal

Structure Database (ICSD).³⁸ The supercell was obtained by a lattice constant of $a = 7.887$ Å, and a periodically reproduced slab supercell was then applied to simulate the $\gamma\text{-Al}_2\text{O}_3(001)$ surfaces. The stoichiometry of the slab is restricted to Al_2O_3 , with 32 aluminum and 48 oxygen atoms. The simulation cell dimensions were fixed to $a = b = 11.15$ Å, $c = 24.02$ Å, and $\alpha = \beta = \gamma = 90^\circ$, including three Al–O layers and two tetrahedral Al layers. The top two floors up and down are symmetrical. The vacuum region was set to 20 Å to separate the slabs in the direction perpendicular to the surface. For the optimization of the adsorption site, both the adsorbed Pt_n cluster and all atoms of the uppermost layer of the $\gamma\text{-Al}_2\text{O}_3$ support were relaxed, whereas the remaining atoms of the support were fixed. The charge transfer was calculated using the Hirshfeld method.³⁹ The electron density difference was computed using the CASTEP program available in Materials Studio 7.0 package.⁴⁰ To gain insight into the metal–metal stabilizing interactions of Pt_n on the $\gamma\text{-Al}_2\text{O}_3(001)$ substrate, the binding energy (E_{BE}) per Pt is defined by using eq i

$$E_{\text{BE}} = \frac{1}{n}(E_{\text{Pt}_n/\text{Al}_2\text{O}_3} - E_{\text{Al}_2\text{O}_3} - nE_{\text{Pt}}) \quad (\text{i})$$

where $E_{\text{Pt}_n/\text{Al}_2\text{O}_3}$ is the energy of the $\text{Pt}_n/\text{Al}_2\text{O}_3$ heterostructure in the optimum geometry, $E_{\text{Al}_2\text{O}_3}$ is the energy of the pristine $\gamma\text{-Al}_2\text{O}_3(001)$, and E_{Pt} is the energy of an isolated Pt atom in the ground triplet state. In this expression of the binding energy, the negative values of E_{BE} indicate stable adsorption configurations.

The energy (E_{MS}) of the metal–slab stabilizing interactions is computed by using eq ii

$$E_{\text{MS}} = E_{\text{BE}} - \Delta E_{\text{def},\text{Al}_2\text{O}_3} - \Delta E_{\text{bond},\text{Pt}_n} \quad (\text{ii})$$

where the second term $\Delta E_{\text{def},\text{Al}_2\text{O}_3}$ (positive) measures the $\gamma\text{-Al}_2\text{O}_3(001)$ deformation energy, defined as the energy penalty to deform $\gamma\text{-Al}_2\text{O}_3(001)$ into the structure adopted in the bonding configuration, by using eq iii

$$\Delta E_{\text{def},\text{Al}_2\text{O}_3} = E_{\text{def},\text{Al}_2\text{O}_3} - E_{\text{Al}_2\text{O}_3} \quad (\text{iii})$$

and the third term $\Delta E_{\text{bond},\text{Pt}_n}$ (negative) is defined as the energy gain owing to the metal–metal bonds by using eq iv

$$\Delta E_{\text{bond},\text{Pt}_n} = \frac{1}{n}(E_{\text{Pt}_n} - nE_{\text{Pt}}) \quad (\text{iv})$$

where E_{Pt_n} is the lowest Pt_n cluster in energy on the surface.

The average cohesive energy, E_{CE} , for the Pt_n cluster in the gas phase is estimated by using eq v

$$E_{\text{CE}} = \frac{1}{n}E_{\text{Pt}_n}^{\text{g}} - E_{\text{Pt}} \quad (\text{v})$$

where $E_{\text{Pt}_n}^{\text{g}}$ is the total energy of the Pt_n cluster in the gas phase and E_{Pt} is the total energy of a single Pt atom.

In addition, the Pt_n cluster deformation energy ($\Delta E_{\text{def},\text{Pt}_n}$), which is associated with the deformation in the structure of the Pt_n cluster between the gas phase and the adsorbed state, is characterized by using eq vi

$$\Delta E_{\text{def},\text{Pt}_n} = E_{\text{Pt}_n} - E_{\text{Pt}_n}^{\text{g}} \quad (\text{vi})$$

Furthermore, to better understand the nucleation or growth of Pt_n clusters on the $\gamma\text{-Al}_2\text{O}_3(001)$ substrate, the nucleation energy (E_{nuc}), which is the energy gained (or lost) in

combining an adsorbed monomer with a Pt_{n-1} cluster to form a Pt_n cluster, is defined as follows

$$E_{\text{nuc}} = E_{\text{Pt}_n/\text{Al}_2\text{O}_3} + E_{\text{Al}_2\text{O}_3} - E_{\text{Pt}_{n-1}/\text{Al}_2\text{O}_3} - E_{\text{Pt}_1/\text{Al}_2\text{O}_3} \quad (\text{vii})$$

■ ASSOCIATED CONTENT

Supporting Information

The Supporting Information is available free of charge on the ACS Publications website at DOI: [10.1021/acsomega.7b00342](https://doi.org/10.1021/acsomega.7b00342).

Total energies, stable configurations, DOS, and the corresponding contour plots of the differential charge density for $\text{Pt}_n/\gamma\text{-Al}_2\text{O}_3(001)$ ([PDF](#))

■ AUTHOR INFORMATION

Corresponding Author

*E-mail: huaqingyang@scu.edu.cn. Fax: 028-85415608. Phone: 028-85415608 (H.-Q.Y.).

ORCID

Hua-Qing Yang: [0000-0002-2985-0389](https://orcid.org/0000-0002-2985-0389)

Chang-Wei Hu: [0000-0002-4094-6605](https://orcid.org/0000-0002-4094-6605)

Author Contributions

The manuscript was written through contributions of all authors. Y.W. was responsible for main computation, B.X. was responsible for part of the computation, H.-Q.Y. was responsible for design, analysis, and writing, and C.-W.H. was responsible for design and revision. All authors have given approval to the final version of the manuscript.

Notes

The authors declare no competing financial interest.

■ ACKNOWLEDGMENTS

The authors are grateful for the financial support by the National Natural Science Foundation of China (grant no.: 21573154) and the Applied Foundation Research of Sichuan Province (grant no.: 2014JY0218).

■ REFERENCES

- (1) Labinger, J. A.; Bercaw, J. E. Understanding and exploiting C–H bond activation. *Nature* **2002**, *417*, 507–514.
- (2) Vajda, S.; Pellin, M. J.; Greeley, J. P.; Marshall, C. L.; Curtiss, L. A.; Ballentine, G. A.; Elam, J. W.; Catillon-Mucherrie, S.; Redfern, P. C.; Mahmood, F.; Zapol, P. Subnanometre platinum clusters as highly active and selective catalysts for the oxidative dehydrogenation of propane. *Nat. Mater.* **2009**, *8*, 213–216.
- (3) Roithová, J.; Schröder, D. Selective activation of alkanes by gas-phase metal ions. *Chem. Rev.* **2010**, *110*, 1170–1211.
- (4) Trevor, D. J.; Cox, D. M.; Kaldor, A. Methane activation on unsupported platinum clusters. *J. Am. Chem. Soc.* **1990**, *112*, 3742–3749.
- (5) Cui, Q.; Musaev, D. G.; Morokuma, K. Molecular orbital study of H_2 and CH_4 activation on small metal clusters. I. Pt, Pd, Pt_2 , and Pd_2 . *J. Chem. Phys.* **1998**, *108*, 8418–8428.
- (6) Cui, Q.; Musaev, D. G.; Morokuma, K. Molecular orbital study of H_2 and CH_4 activation on small metal clusters. 2. Pd_3 and Pt_3 . *J. Phys. Chem. A* **1998**, *102*, 6373–6384.
- (7) Xiao, L.; Wang, L. Methane Activation on Pt and Pt_4 : A Density Functional Theory Study. *J. Phys. Chem. B* **2007**, *111*, 1657–1663.
- (8) Li, F.-M.; Yang, H.-Q.; Ju, T.-Y.; Li, X.-Y.; Hu, C.-W. Activation of C–H and C–C bonds of ethane by gas-phase Pt atom: potential energy surface and reaction mechanism. *Comput. Theor. Chem.* **2012**, *994*, 112–120.
- (9) Li, F.-M.; Yang, H.-Q.; Ju, T.-Y.; Li, X.-Y.; Hu, C.-W. Activation of propane C–H and C–C bonds by gas-phase Pt atom: a theoretical study. *Int. J. Mol. Sci.* **2012**, *13*, 9278–9297.
- (10) Ju, T.-Y.; Yang, H.-Q.; Li, F.-M.; Li, X.-Y.; Hu, C.-W. Reaction mechanism on the activation of ethane C–H and C–C bonds by a diplatinum cluster. *Theor. Chem. Acc.* **2013**, *132*, 1387.
- (11) Ju, T.-Y.; Yang, H.-Q.; Li, F.-M.; Li, X.-Y.; Hu, C.-W. Activation of propane C–H and C–C bonds by a diplatinum cluster: potential energy surfaces and reaction mechanisms. *Struct. Chem.* **2014**, *25*, 471–481.
- (12) Fu, H.-Q.; Su, B.-F.; Yang, H.-Q.; Hu, C.-W. Theoretical insight into the C–H and C–C scission mechanism of ethane on a tetrahedral Pt_4 subnanocluster. *RSC Adv.* **2015**, *5*, 40978–40988.
- (13) Zhou, C.; Wu, J.; Kumar, T. J. D.; Balakrishnan, N.; Forrey, R. C.; Cheng, H. Growth pathway of Pt clusters on $\alpha\text{-Al}_2\text{O}_3(0001)$ surface. *J. Phys. Chem. C* **2007**, *111*, 13786–13793.
- (14) Mei, D.; Kwak, J. H.; Hu, J.; Cho, S. J.; Szanyi, J.; Allard, L. F.; Peden, C. H. F. Unique role of anchoring penta-coordinated Al^{3+} sites in the sintering of $\gamma\text{-Al}_2\text{O}_3$ -supported Pt catalysts. *J. Phys. Chem. Lett.* **2010**, *1*, 2688–2691.
- (15) Liu, Y.; Cen, W.; Feng, G.; Chu, Y.; Kong, D.; Yin, H. First principles study on the adsorption of Pt_n ($n = 1$ –4) on $\gamma\text{-Al}_2\text{O}_3(110)$ surface. *Appl. Surf. Sci.* **2014**, *313*, 424–431.
- (16) Han, Y.; Liu, C.-j.; Ge, Q. Interaction of pt clusters with the anatase $\text{TiO}_2(101)$ surface: a first principles study. *J. Phys. Chem. B* **2006**, *110*, 7463–7472.
- (17) Gong, X.-Q.; Selloni, A.; Dulub, O.; Jacobson, P.; Diebold, U. Small Au and Pt clusters at the anatase $\text{TiO}_2(101)$ surface: behavior at terraces, steps, and surface oxygen vacancies. *J. Am. Chem. Soc.* **2008**, *130*, 370–381.
- (18) Zhou, Y.; Muhich, C. L.; Neltner, B. T.; Weimer, A. W.; Musgrave, C. B. Growth of Pt particles on the anatase $\text{TiO}_2(101)$ surface. *J. Phys. Chem. C* **2012**, *116*, 12114–12123.
- (19) Jiang, D.-e.; Overbury, S. H.; Dai, S. Structures and energetics of Pt clusters on TiO_2 : interplay between metal–metal bonds and metal–oxygen bonds. *J. Phys. Chem. C* **2012**, *116*, 21880–21885.
- (20) Li, Y.; Gao, W.; Ci, L.; Wang, C.; Ajayan, P. M. Catalytic performance of Pt nanoparticles on reduced graphene oxide for methanol electro-oxidation. *Carbon* **2010**, *48*, 1124–1130.
- (21) Okazaki-Maeda, K.; Morikawa, Y.; Tanaka, S.; Kohyama, M. Structures of Pt clusters on graphene by first-principles calculations. *Surf. Sci.* **2010**, *604*, 144–154.
- (22) Qiu, J.-D.; Wang, G.-C.; Liang, R.-P.; Xia, X.-H.; Yu, H.-W. Controllable deposition of platinum nanoparticles on graphene as an electrocatalyst for direct methanol fuel cells. *J. Phys. Chem. C* **2011**, *115*, 15639–15645.
- (23) Lim, D.-H.; Wilcox, J. DFT-based study on oxygen adsorption on defective graphene-supported Pt nanoparticles. *J. Phys. Chem. C* **2011**, *115*, 22742–22747.
- (24) Aranifard, S.; Ammal, S. C.; Heyden, A. Nature of $\text{Pt}_n/\text{CeO}_2(111)$ surface under water–gas shift reaction conditions: A constrained ab initio thermodynamics study. *J. Phys. Chem. C* **2012**, *116*, 9029–9042.
- (25) Xu, D.; Liu, Y.-J.; Zhao, J.-X.; Cai, Q.-H.; Wang, X.-Z. Theoretical study of the deposition of Pt clusters on defective hexagonal boron nitride (h-BN) sheets: morphologies, electronic structures, and interactions with O. *J. Phys. Chem. C* **2014**, *118*, 8868–8876.
- (26) Digne, M.; Sautet, P.; Raybaud, P.; Euzen, P.; Toulhoat, H. Hydroxyl groups on $\gamma\text{-Alumina}$ surfaces: a DFT study. *J. Catal.* **2002**, *211*, 1–5.
- (27) Digne, M.; Sautet, P.; Raybaud, P.; Euzen, P.; Toulhoat, H. Use of DFT to achieve a rational understanding of acid–basic properties of $\gamma\text{-alumina}$ surfaces. *J. Catal.* **2004**, *226*, 54–68.
- (28) Valero, M. C.; Raybaud, P.; Sautet, P. Influence of the hydroxylation of $\gamma\text{-Al}_2\text{O}_3$ surfaces on the stability and diffusion of single Pd atoms: a DFT study. *J. Phys. Chem. B* **2006**, *110*, 1759–1767.

- (29) Pinto, H. P.; Nieminen, R. M.; Elliott, S. D. Ab initio study of γ -Al₂O₃ surfaces. *Phys. Rev. B: Condens. Matter Mater. Phys.* **2004**, *70*, 125402.
- (30) Ouyang, C. Y.; Šljivančanin, Ž.; Baldereschi, A. First-principles study of γ -Al₂O₃(100) surface. *Phys. Rev. B: Condens. Matter Mater. Phys.* **2009**, *79*, 235410.
- (31) Chen, Y.; Ouyang, C.; Shi, S.; Sun, Z.; Song, L. Density functional theory study of Ir atom deposited on γ -Al₂O₃ (001) surface. *Phys. Lett. A* **2009**, *373*, 277–281.
- (32) Nasluzov, V. A.; Shulimovich, T. V.; Shor, A. M.; Bukhtiyarov, V. I.; Rösch, N. Small gold species supported on alumina. a computational study of α -Al₂O₃(0001) and γ -Al₂O₃(001) using an embedded-cluster approach. *Phys. Status Solidi B* **2010**, *247*, 1023–1031.
- (33) Allis, D. G.; Prokhorova, D. A.; Korter, T. M. Solid-State modeling of the terahertz spectrum of the high explosive HMX. *J. Phys. Chem. A* **2006**, *110*, 1951–1959.
- (34) Perdew, J. P.; Wang, Y. Accurate and simple analytic representation of the electron-gas correlation energy. *Phys. Rev. B: Condens. Matter Mater. Phys.* **1992**, *45*, 13244–13249.
- (35) Delley, B. An all-electron numerical method for solving the local density functional for polyatomic molecules. *J. Chem. Phys.* **1990**, *92*, 508–517.
- (36) Delley, B. From molecules to solids with the Dmol₃ approach. *J. Chem. Phys.* **2000**, *113*, 7756–7764.
- (37) Bergner, A.; Dolg, M.; Küchle, W.; Stoll, H.; Preuß, H. Ab initio energy-adjusted pseudopotentials for elements of groups 13–17. *Mol. Phys.* **1993**, *80*, 1431–1441.
- (38) Gutiérrez, G.; Taga, A.; Johansson, B. Theoretical structure determination of γ -Al₂O₃. *Phys. Rev. B: Condens. Matter Mater. Phys.* **2001**, *65*, 012101.
- (39) Hirshfeld, F. L. Bonded-atom fragments for describing molecular charge densities. *Theor. Chim. Acta* **1977**, *44*, 129–138.
- (40) Seidl, A.; Görling, A.; Vogl, P.; Majewski, J. A.; Levy, M. Generalized Kohn-Sham schemes and the band-gap problem. *Phys. Rev. B: Condens. Matter Mater. Phys.* **1996**, *53*, 3764–3774.
- (41) Perdew, J. P.; Chevary, J. A.; Vosko, S. H.; Jackson, K. A.; Pederson, M. R.; Singh, D. J.; Fiolhais, C. Atoms, molecules, solids, and surfaces: applications of the generalized gradient approximation for exchange and correlation. *Phys. Rev. B: Condens. Matter Mater. Phys.* **1992**, *46*, 6671–6687.
- (42) Ankudinov, A. L.; Rehr, J. J.; Low, J. J.; Bare, S. R. Sensitivity of Pt X-ray absorption near edge structure to the morphology of small Pt clusters. *Chem. Phys.* **2002**, *116*, 1911–1919.
- (43) Frenkel, A. I.; Hills, C. W.; Nuzzo, R. G. A view from the inside: complexity in the atomic scale ordering of supported metal nanoparticles. *J. Phys. Chem. B* **2001**, *105*, 12689–12703.
- (44) Saidi, W. A. Density Functional theory study of nucleation and growth of Pt nanoparticles on MoS₂(001) surface. *Cryst. Growth Des.* **2015**, *15*, 642–652.
- (45) Liu, X.; Li, L.; Meng, C.; Han, Y. Palladium Nanoparticles/Defective Graphene Composites as Oxygen Reduction Electrocatalysts: A First-Principles Study. *J. Phys. Chem. C* **2012**, *116*, 2710–2719.
- (46) Lim, D.-H.; Wilcox, J. Mechanisms of the Oxygen Reduction Reaction on Defective Graphene-Supported Pt Nanoparticles from First-Principles. *J. Phys. Chem. C* **2012**, *116*, 3653–3660.
- (47) Fampiou, I.; Ramasubramaniam, A. Binding of Pt Nanoclusters to Point Defects in Graphene: Adsorption, Morphology, and Electronic Structure. *J. Phys. Chem. C* **2012**, *116*, 6543–6555.